World Academy of Science, Engineering and Technology
International Journal of Physical and Mathematical Sciences
Vol:8, No:9, 2014

Investigation of the GFR2400 Reactivity Control System

Ján Haščík, Štefan Čerba, Jakub Lüley, Branislav Vrban

***Abstract*—**The presented paper is related to the design methods and neutronic characterization of the reactivity control system in the large power unit of Generation IV Gas cooled Fast Reactor – GFR2400. The reactor core is based on carbide pin fuel type with the application of refractory metallic liners used to enhance the fission product retention of the SiC cladding. The heterogeneous design optimization of control rod is presented and the results of rods worth and their interferences in a core are evaluated. In addition, the idea of reflector removal as an additive reactivity management option is investigated and briefly described.

***Keywords*—**Control rods design, GFR2400, hot spot, movable reflector, reactivity.

I. Introduction

GENERATION IV International Forum (GIF) is a cooperative international endeavor that is currently trying to define and perform research and development needed to establish feasibility and performance capabilities of the next generation of nuclear energy systems. The GIF Technology Roadmap [1] identified the Gas-cooled Fast Reactor (GFR) as a challenging and innovative idea that is one of the best options from the sustainability point of view with ability of minor actinides transmutation, high potential heat generation and a possibility to work with closed fuel cycle. The GFR is a fast neutron spectrum system that must be seen as a complement and alternative to the SFR deployment, which benefits from a more mature technology [2].

The GFR2400 reactor is considered as a conceptual design of a large scale power GFR. This design is based on the foregoing concepts and experiences of all the GoFastR participants. In European FP7, the GoFastR project was the Euratom contribution to the Gen IV gas cooled fast reactors (GFR).The GFR2400 design is featuring ceramic fuel and structural materials both allowing high temperatures and efficiency using helium coolant. An important innovation of the current design is the application of refractory metallic liners used to enhance the fission product retention of the cladding, resulting in a significant neutronic penalty during normal operation and at the same time being advantageous under transient conditions involving spectrum softening [3].

J. Haščík is with the Institute of Nuclear and Physical Engineering, Slovak University of Technology in Bratislava, Ilkovičova 3, 812 19, Bratislava, Slovakia, EU (phone: +421-2-602-91-289; fax: +421-2-6542-7207; e-mail: jan.hascik@stuba.sk).

Š. Čerba, J. Lüley, and B. Vrban were with KAERI, Daejeon, South Korea. They are now with the Institute of Nuclear and Physical Engineering, Slovak University of Technology in Bratislava, Ilkovičova 3, 812 19, Bratislava, Slovakia, EU (e-mail: stefan.cerba@stuba.sk, jakub.luley@stuba.sk, branislav.vrban@stuba.sk).

Either fast or thermal reactor systems may benefit from the system of a partially moveable reflector incorporated in the design, since the significant adjustable leaks of neutrons may be used to control reactivity in case of accident managing. Especially in a fast neutron spectrum, due to the smaller transport cross-section, the migration area of neutrons is exceptionally large. Thus the possibility of reactivity control by the movable reflector appears to be a promising additional safety solution. In this paper we present the results of a neutronic study of the GFR2400 reactor core design based on GoFastR documents [4]. Due to the fact that no final design of control rods is available, the heterogeneous design of control rods is proposed and the used methodology is described. In addition, the worth of control rods at several insertions coupled with the reflector positions were investigated, the shadowing and anti-shadowing effects were calculated for heterogeneous and homogenous control rod design and the influence of new control rod design to identified hot spots (described in detail in our foregoing work [5]) were assessed. In our previous analyses all the calculations were performed just with the homogenous control rods designs so the new heterogeneity effects were studied and are described in this paper.

II. Geometry And Material Description

A. General Design Overview

The GFR2400 design is a large scale power unit with thermal power of 2400 MW_{th}. This fast-spectrum reactor is a helium-cooled system and it works with a closed fuel cycle. Primary coolant pressure during normal operation reaches 7 MPa in order to ensure adequate heat transfer. Due to the safety reasons, the coolant volume fraction in a core is rather high. This fact allows maintaining the natural circulation of a coolant under pressurized conditions even if active systems are not available. The three decay heat removal loops (each 100% capacity) with heat exchangers and forced convection devices are available and the six additional gas reservoirs are prepared in case of emergency to mitigate the core melting accident. The global primary arrangement is based on three main loops (3×800 MW_{th}), each fitted with one IHX blower unit, enclosed in a single vessel. The current choice of power conversion system is the indirect Brayton cycle working with the He-N_2 mixture. The planed cycle efficiency is approximately 45%. The GFR2400 system main characteristic parameters including inlet and outlet coolant temperatures and working pressures are given in the Table I:

TABLE I
GENERAL DESIGN PARAMETERS [3]

Parameter	value	unit
Thermal power	2400	MW_{th}
Primary pressure	7	MPa
Mass flow rate	1213	kg/s
Core inlet temp.	400	°C
Core pressure drop	0.143	MPa
Core outlet temp.	780	°C
Secondary pressure	6.5	MPa

Due to the fact that components of GFR2400 need to withstand high temperatures, ceramic compositions are under investigation as a promising solution for the used materials. The pin fuel of active length of 165cm consists of uranium plutonium carbide (UPuC) surrounded by tungsten-rhenium compound (W14Re) and rhenium (Re) refractory liners to ensure fission products confinement within the pins. The gap between fuel and liners is filled with helium gas with the pressure of 1MPa. The use of a SiCf/SiC material for fuel cladding is the latest and very promising solution, where the SiC fibers are improving mechanical properties [6].

The active core consists of two zones. The PuC volumetric content in the inner core (IC) fuel assemblies (FA) reaches 14.2%, and 17.6% in the outer core (OC) The isotopic composition of uranium corresponds with the natural uranium whereas plutonium composes of the twice recycled mixed oxide (MOX) fuel expected to be available in France since 2016[7].The core fuel region is surrounded by six rings of Zr_3Si_2 reflector assemblies in the radial direction and by the 1m high axial reflectors of the same material placed above and below the fission gas plenums. A general view of the GFR core can be found in Fig. 1.

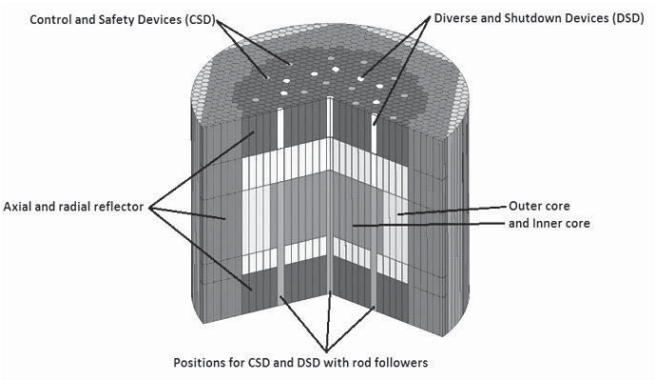

Fig. 1 3D cross-sectional view of GFR2400 reactor model

The inner part consists of 264 and the outer one of 252 fuel assemblies. The control rod (CR) system is composed of 13 Diverse Safety Devices (DSD) and 18 Control and Safety Devices (CSD) with the same material composition of B_4C (90% of ^{10}B). The rod follower is made of a structural material (containing SiC) which was also implemented into the calculation model. Additional tabulated geometrical data are presented in Table II.

TABLE II
THE MAIN GFR2400 CORE PARAMETERS [3]

region	parameter	value	unit
Fuel assembly	Pin radius	3.335	mm
	Fuel gap radius	3.5	mm
	W14Re liner radius	3.354	mm
	Re liner radius	3.55	mm
	Clad radius	4.55	mm
	SiC liner radius	0.458	mm
	Lattice pitch	11.57	mm
	Wrapper thickness	2	mm
	Wrapper outside	8.7645	cm
	S/A pitch	8.9145	cm
	No. of pins in FA	217	pcs
Core	FA	516	pcs
	CSD	18	pcs
	DSD	13	pcs
	Reflector	480	pcs

B. Calculation Model Specification

The 3D hexagonal models of GFR2400 MW_{th} core were prepared in the SCALE [8]and in MCNP5 [9]calculation code systems based on the carbide fuel pin type core design available in GoFastR internal documents[4]. The IC & OC fuel parts are modelled heterogeneously with respect to all the dimensions presented in Table II. Fuel pins were modelled with a temperature of 1263 K. The tungsten and tungsten-rhenium liners were modelled with a common temperature 913 K. The radial and axial reflector parts (non-fuel regions) were modelled homogeneously according to the internal specification. The 60% of upper and lower reflector volume was filled with Zr_3Si_2 material and the remaining portion was the helium gas of 7 MPa. In the radial reflector 80% of volume was Zr_3Si_2 and the rest was filled with a helium gas. Finally the composition of CSD and DSD rods is as follows: absorber B_4C – 30.26%, structural material AIM1 11.22%, SiC 10.85% and He gas pressurized to 7 MPa 47.67%. Associated homogeneous rod follower composition is specified as: AIM1 1.20%, SiC 10.85% and He (7 MPa) 87.95%.

As was already mentioned no final design of control rod was proposed for GFR2400 pin design. Interesting results can be found in [10], where the control rod for GFR plate design is introduced. However neutronic situation of pin core is obviously different thus our own approach is introduced in the further sections.

III. COMPUTATIONAL TOOLS

For this analysis these two computational systems were used: MCNP5 v1.6 and SCALE 6.1.2. Both have their own advantages and together they are able to cover the investigated attributes.

SCALE is a comprehensive modelling and simulation suite for nuclear safety analysis and design that is developed, maintained, tested and managed by the Reactor and Nuclear Systems Division (RNSD) of Oak Ridge National Laboratory (ORNL). The KENO-VI module was chosen as a Monte Carlo criticality program used to calculate k_{eff} of three-dimensional systems and other quantities including lifetime, generation

time, energy-dependent leakages, energy and region dependent absorptions, fissions, flux densities and fission densities.

All the KENO-VI calculations were performed using the 238 group ENDF/B VII.0 data libraries except one case where the continues data library was used to evaluate computational difference of KENO-VI and MCNP5. Computational sequence CENTRM/PMC was used to generate problem depended self-shielded multigroup (MG) cross sections. CENTRM computes continuous-energy neutron spectra using deterministic approximations to the Boltzman transport equation in one-dimensional or infinite media geometry. PMC process CENTRM continuous-energy flux spectra and cross section data to problem depended multigroup library. To include all the resonances of materials occurring in the fuel pin lattice, the upper range of continues-energy calculation in CENTRM was extended to 800 keV.

MCNP is a general-purpose Monte Carlo N–Particle code that can be used for neutron, photon, electron, or coupled neutron/photon/electron transport, including the capability to calculate eigenvalues for critical systems. The code treats an arbitrary three-dimensional configuration of materials in geometric cells. Pointwise cross-section data are used. Important standard features that make MCNP very versatile and easy to use include a powerful general source, criticality source, and surface source; both geometry and output tally plotters; a rich collection of variance reduction techniques a flexible tally structure and an extensive collection of cross-section data. For the MCNP5 calculations presented in this paper continuous energy (CE) ENDF/B VII.0 data libraries were prepared using the NJOY99 [11] code. Taking into account that MCNP uses continues energy data libraries and KENO-VI uses MG method, the agreement between the two codes can be concluded as satisfactory.

IV. Definition of the Calculation Cases

The initial state of the reactor is in this paper defined as a reactor in nominal operation conditions, where all the structural materials, fuel and coolant have nominal temperature presented in the model specification paragraph. The CSDs and DSDs are positioned in the upper edge of the fuel, at position h=165cm (marked as "All up"). For the initial state Doppler and void coefficient's calculations were performed, where in the Doppler case the fuel temperature was changed to T_D = 2273 K, which is a limit exceeding the critical temperature of cladding failure [12]. In the void case the nominal pressure of the coolant varied in the range from P_N = 70 bar to P_V = 1 bar. The calculation parameters are summarized in Table III.

TABLE III
Parameters for the Void and Doppler Effects

State	Fuel T (K)	Structural materials T (K)	Coolant P (bar)	CSD, DSD position h (cm)
Nominal	1263	913	70	165
Void	1263	913	1	165
Doppler	2273	913	70	165

Since no final heterogeneous design of the control rod has been made so far, a design approach was proposed and a simple heterogeneous control rod design was developed. The effectiveness evaluation of the proposed heterogeneous control rod design is based on calculation of the worth of the given device and compared with the basic homogenous design. The worth of the CSD and DSD devices was investigated for simple devices as well as for a given group configurations. Due to the one-sixth symmetry of the reactor core, only unique devices were investigated separately. The investigated devices were fully inserted at the given position in the reactor core. This position corresponds with bottom edge of the fuel. This case was marked as "All down". The applied numbering system for CSD and DSD devices is shown in Fig. 2.

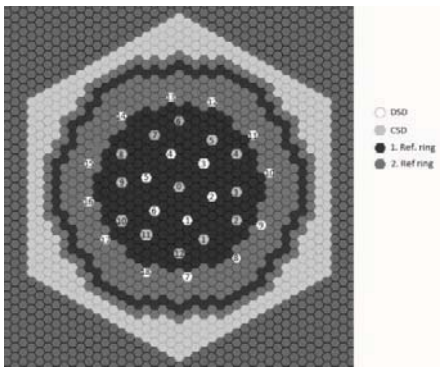

Fig. 2 The applied numbering system of CSD and DSD devices

The reactivity worth was calculated for single CSD 2,3,10,11 and DSD 0,4,5 devices; for the first (device 1-6) and second (device 7-18) ring of CSD devices and for the whole configuration of CSD and DSD devices. For the selected homogenous and heterogeneous assemblies also the interference from other devices was investigated through the calculation of amplification factors. Apart from the calculation of the worth of control rods, the worth of withdrawn reflector assemblies was investigated as well, as an alternative option for accidental reactivity management. Various reflector assembly configurations were studied. However, only the most promising ones are presented in this paper.

The removed assemblies were dropped to the lower edge of the fuel part and the investigation was performed based on local multiplication fraction (*LMF*) results, in conjunction with the neutron fluxes and the overall worth of the removed reflector assemblies. The definition of *LMF* from the SCALE manual is based on calculation of the fission production matrix by the subroutine MATRIX and this parameter represents the multiplication capabilities of each investigated S/A. The fission production matrix is defined as the number of next-generation neutrons produced at position index *J* per neutron born at position index *I*. Finally the collection and summation of fission production matrices from all the positions over the investigated source position represents our *LMF* [8]. Two configurations are presented, the reactivity worth of the

removal of the first and of the second ring of reflector assemblies around the core.

V. Development of Simple Heterogeneous CR Design

A. Single-Pin Calculation

In every control rod design the assessment of the optimal pin radius should be an important consideration. If the radius is too large, the absorber material is not utilized in the most effective way, due to self-shielding. In terms of neutronics, an appropriate way to find the optimal pin radius may be obtained through the investigation of the neutron penetration distance, performed on a simple absorber pin. A one-pin design is a semi 1D approach, which prevents any interference caused by the self-shielding or geometrical influences of the surrounding absorber pins. On the basis of the homogenous material composition of the control rods described in the calculation model specification a simple pin design was created. In this simple model the radius of the absorber pin and the clad were calculated to keep the volume fractions of all the materials from the homogenous compositions. The top view of the cross-section of the single-pin absorber assembly is shown in Fig. 3.

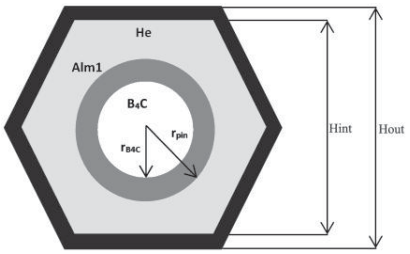

Fig. 3 The cross section of the single-pin design control mechanism

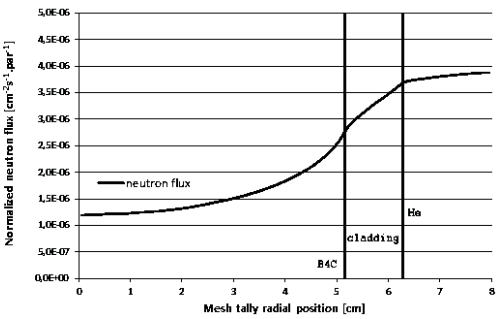

Fig. 4 Neutron flux results of the single-pin control mechanism

The radius of the B_4C absorber was calculated to 5.16 cm while the total radius of the pin including the cladding and the void space between the clad and the absorber was 6.28 cm. The outer wrapper of the absorber S/As was made of SiC structure and the remaining part of the assembly was filled with helium coolant at a 70 bar pressure. The absorber assembly was fully inserted into the central DSD0 channel of the presented GFR2400 ceramic pin core, while the remaining CSD and DSD assemblies were set to the upper parking position. A steady state Monte Carlo criticality calculation was performed and to assess the energy integral neutron flux as a function of pin radius, fine cylindrical neutron mesh tallies were used with the step of 1 mm. The plot of the results is shown in Fig. 4.

The results clearly show that a linear-like decrease of the neutron flux can be observed in the cladding region. In the outer region of the B_4C absorber, the flux is degraded rapidly but towards the central part of the absorber pin, the slope is decreasing and in the region between 0 and 2 cm there is almost no change of the neutron flux. This phenomenon can be explained by the geometric self-shielding of the neutron flux; thus the radius of the investigated absorber pin is significantly higher than the penetration distance of the neutrons in the absorber. Therefore, the ^{10}B atoms in the central part of the pin have no reasonable chance for neutron capture. The comparison of the neutron flux in different positions showed that a pin radius of 2.8 cm would be appropriate to decrease the neutron flux by the value of two. The mean free path of neutrons in B_4C was calculated to 2.56 cm.

In the real control rod designs the absorber pins are organized in a hexagonal S/As in a ring-wise configuration. It is assumed that the movement of the reactivity control system is ensured using a rod follower mechanism, placed at the central part of the absorber assembly. In order to limit the possible radiation damage caused by the fluence of fast neutrons on the driver mechanism a central wrapper is introduced between the rod follower and the absorber pins.

If we consider a constant mass of the absorber material, the constant absorber pin height, the pitch of absorber pins p_{abs}defined by (1) then the number of absorber pins N_{pin}can be calculated by (2) and the radius of the absorber pin $r_{abs}$by (3).

$$p_{abs} = \frac{H_{int}}{\overline{3}\ 2N_{rings}-1} \quad (1)$$

$$N_{pin} = 1 + \sum_{i=0}^{N_{rings}-1} 6i \quad (2)$$

$$r_{abs} = \sqrt{\frac{\frac{V_{abs}}{N_{pin}}}{\pi.h_{pin}}} \quad (3)$$

In the equations H_{int} is the across flat of the internal S/As wrapper, $N_{rings}$the number of rings, V_{abs} the total volume of the absorber material and $h_{pin}$is the height of the absorber pin. The results of the pin radii can be found in Table IV. For each value the relative position from the boundary between the absorber and the cladding of the single pin model was calculated. This value represents a hypothetical case determining the effectiveness of the absorber pin of a given radius for neutron absorption. (For example, in case of 1 ring design there are 6 absorber pins with a radius of 2.56 cm. In this case the distance from the boundary between the absorber and the cladding is 5.15-2.56=2.59 cm.) For each position the corresponding values of the neutron flux, obtained from the mesh tally results, were compared. For this purpose three comparative coefficients have been introduced. The C_1

coefficient was calculated using (4) and it represents the ratio of the neutron flux $\varphi_i$at the given position to the flux at the boundary between the absorber and the claddingφ_0. The lower the C_1 coefficient is, the higher the flux depression is.

$$C_1 = \frac{\varphi_i}{\varphi_0} \quad (4)$$

The C_1 coefficient represents only the depression of the neutron flux caused by the introduction of a neutron absorber of a given radius. To evaluate the effectiveness of the absorber per unity of thickness the C_2 coefficient was used. This can be calculated by means of (5). In terms of neutron flux depression, the higher the C_2 value, the more efficient the unity of a given material.

$$C_2 = \frac{C_1}{r_{abs}} \quad (5)$$

It is obvious that for economic reasons the design of the reactivity control system should be as simple as possible. This leads to a requirement to minimize the number of absorber pins in the S/As. To meet this fact, an additional C_3 coefficient has been introduced. This value modifies the C_2 value to account for the total number of fuel pins per given absorber mass. The C_3 value can be calculated by using (6) and it can be stated that a higher value represents better performance. To keep the range of C_3 between 1 and 100, it was multiplied by 1.E3.

$$C_3 = \frac{1E3.C_2}{N_{pin}} \quad (6)$$

TABLE IV
RESULTS OF THE SINGLE PIN CALCULATION

Rings	Pins	r_{pin} [cm]	Pos. [cm]	φ [$cm^{-2}s^{-1}par^{-1}$]	C_1	C_2	C_2
0	0	5.15	0.00	2.76E-06	-	-	-
2	7	2.563	2.59	1.43E-06	0.517	0.202	28.82
3	19	1.812	3.34	1.60E-06	0.581	0.320	16.87
4	37	1.146	4.00	1.84E-06	0.667	0.582	15.73
5	61	0.854	4.30	1.98E-06	0.719	0.842	13.80
6	91	0.740	4.41	2.05E-06	0.742	1.003	11.02
7	127	0.604	4.55	2.13E-06	0.773	1.279	10.07
8	169	0.513	4.64	2.20E-06	0.797	1.555	9.20
9	217	0.468	4.68	2.23E-06	0.810	1.730	7.97
10	271	0.410	4.74	2.28E-06	0.826	2.013	7.43

As it was mentioned, the C_1 and C_2coefficients are useful to compare the various radii of the control rod in terms of effectiveness of neutron flux depression, while C_3 is used for economic reasons. To account for both neutronic and economic effectiveness the C_2 and C_3 coefficients were graphically compared in Fig. 5. The C_2 coefficient shows the best performance for thin pins; whereas the C_3 coefficient acquires its maximum for pins of large radii. If we make the intersection of the two curves we can find the optimal pin radius. In our case it lies in the region of 5 - 6 rings. Although the 10 ring configuration seems to be the most promising in terms of core neutronic; however, due to economic reasons, the configurations accommodating more than 6 rings are not really preferable.

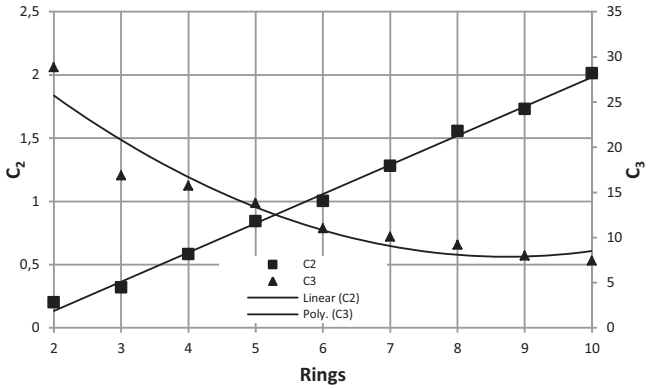

Fig. 5 Comparison of the C_2 and C_3 coefficients Ring-wise calculation

B. Ring- Wise Calculations

To prove our hypothesis from the single-pin calculation, 9 different control rod designs were developed, stretching from 2 to 10 ring configurations. In each case the absorber pins were placed in hexagonal ring-wise structure, while the total volume of the absorber material was kept constant. All CSD and DSD positions were filled with the heterogeneous control devices placed at the bottom core position ("All down") and a steady state criticality calculation was performed for each case. The absolute worth of the control devices was calculated using (7) and it was compared to the worth of the homogenous control device using (8). The results of the control rod worth calculations are shown in Table V.

$$\Delta\rho_i^a = \rho_{AU} - \rho_i \quad (7)$$

$$\Delta\rho_i^r = \frac{\Delta\rho_i^a}{\rho_{homo}} \quad (8)$$

The results demonstrate that the worth of the 2 ring configuration is not appropriate, since the worth of this control device is only 90 % of the homogenous case. The efficiency of the other configurations lies between 93.15% and 94.77%. The graphical plot of the results is showing an upward tendency of the efficiency towards the 10 ring configuration. However, the steepest slope can be observed between 3 and 5 rings. Since the difference of the control devices worth between the 6 and the 10 ring cases is only 18 pcm, while the pin radius in the 10 ring case is the half, it can be concluded that it is not preferable to further investigate a control rod design with more than 5-6 rings.

This is in very a good agreement with the results of the single-pin calculation. Based on the achieved result from the single-pin and ring-wise calculations the configuration with 5 rings of absorber pins has been selected as the basic option. It should be noted, that the final decision can be made only on the basis of additional radiation heating and depletion analyses which have not been a part of this study and will be investigated in the future.

TABLE V
RESULTS OF THE RING CALCULATIONS

Number of rings	Pin radius [cm]	ρ_i [pcm]	$\Delta\rho_i^a$ [pcm]	$\Delta\rho_i^r$ [-]
Homogenous		-10707.6	12538.5	1.0000
2	2.1056	-9469.07	11299.93	0.9012
3	1.4889	-9849.07	11679.92	0.9315
4	0.9417	-9938.43	11769.29	0.9387
5	0.7019	-9968.66	11799.51	0.9411
6	0.6078	-10023.1	11853.96	0.9454
7	0.4963	-10019.5	11850.33	0.9451
8	0.4211	-10015.8	11846.7	0.9448
9	0.3844	-10052.2	11883.02	0.9477
10	0.3372	-10042.5	11873.33	0.9470

C. Investigation of the Influence on the Absorber Pin Pitch

The single-pin calculation was intended to segregate the influence of the shielding effect between the adjacent absorber pins and to point out the self-shielding of the given pin itself. To account for the undisputable interferences between the pins in the absorber S/As additional considerations had to be made. This influence can be found by changing the pitch of the absorber pins in the S/As. This analysis was performed on the 5 ring configuration (hereinafter R5) of the control rod. The pitch varied between 1.9cm and 2.15cm while a steady state criticality calculation was performed with all the control devices fully inserted to the reactor core. Apart from the calculation of the control rod worth the total and the B_4C absorption rates were tallied. The results of the absorption rates for the 1.9cm and 2.15cm cases are shown in Fig. 6.

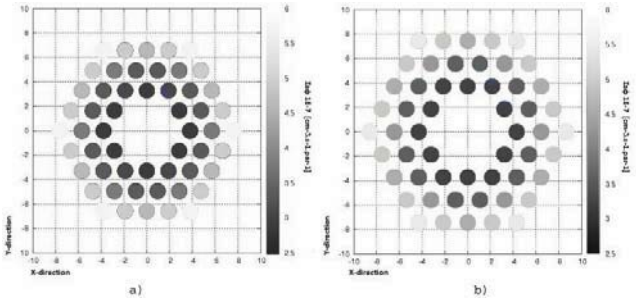

Fig. 6 Results of the absorption rates for various pin pitches

The results are showing a strong interference between the absorber pins which was almost linearly decreasing for lower pin pitches. The difference in the control rod worth between the a) - 1.9cm and the b) - 2.15cm cases was 365 pcm which is approximately 12 pcm per a single S/A. The uncertainty of the Monte Carlo calculation was 8.75 pcm. The B_4C absorption increased by 2.76% and the total absorption of the S/As by 2.8%. The comparison of the 1.9cm and the 2.15cm cases confirmed our expectations. The 1.9 cm cases shows very strong neutron absorption in the outer ring of absorber pins leading to a weakening of the central part of the S/As. Due to the large number density of ^{10}B at the boundary the majority of low and intermediate energy neutrons is absorbed in the outer ring and therefore only the high energy neutrons can reach the central parts of the S/As. Although the absorption in the outer ring in case of the 2.15cm design is less significant, due to the "gaps" between the absorption more neutrons of intermediate energies can reach the central region, leading to flatter absorption distribution across the assembly and higher overall worth.

D. Additional Considerations

Apart from the pitch of the absorber pins, there are several additional elements that could influence the performance of the control device, including the thickness and position of the central wrapper as well. The investigation of the influence of the position and thickness of the central wrapper was investigated using the R5 control rod design with 1.9 cm pitch of the absorber pins. As in the previous case, the focus was on the reactivity worth and on the absorption rates. Not the total absorber rates very tallied however, just the contribution from the neutrons reflected from the central wrapper. This was achieved using the tally flagging feature of the MCNP code. The comparison of the absorption rates for two different central wrapper positions is shown in Fig.7. The position of the central wrapper varied from a) – 3 cm to b) - 4.5 cm. Additional calculations were performed for the 3 cm central wrapper position where its thickness varied from 0.5 to 3 cm.

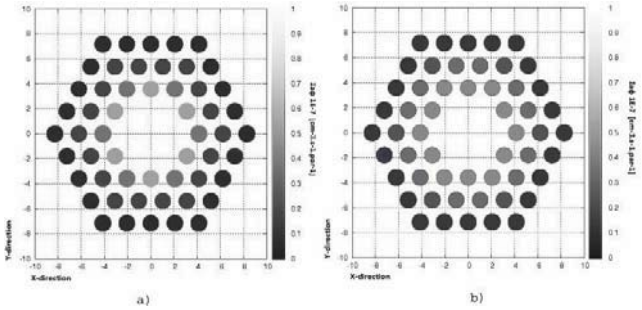

Fig. 7 Results of the absorption rates for various wrapper positions

The results show a noticeable influence on the position of the central wrapper. The smaller the distance between the central wrapper and the absorber pins, the higher the absorption rate of scattered neutrons in the central wrapper. Still; this influence is significant for the central ring of absorber pins only, the absorption rates of the outer were almost the same. The total reactivity worth caused by different wrapper position was only 21 pcm. The calculation with various central wrap thicknesses showed higher reactivity worth, about 68 pcm. The highest assembly worth was achieved in case of 3 cm thick central wrapper; but the highest absorption rate on B_4C was for a 1.5 thick wrapper. This fact can be explained by the increasing capture to scatter rate on the central wrapper.

VI. RESULTS

A. Void, Doppler and Rod Worth Calculations

The results of the Void and Doppler calculations are presented in Table VI. The k_{eff} for each computational state is presented with its related standard deviation and the reactivity calculated as a relative deviation of k_{eff} from one. The Doppler constant (DC) was computed using (9).

$$DC = \frac{\Delta\rho}{ln\frac{T_2}{T_1}} \quad (9)$$

TABLE VI
THE RESULTS OF THE VOID AND DOPPLER CALCULATIONS

Doppler calculation $P_{coolant}$= 70 bar (Nominal T_{fuel} = 1263 K)					
T_{fuel} (K)	k_{eff}	σ_{std}	ρ (pcm)	Δρ (pcm)	DC
2273	1.012937	0.00006	1277.18	-638.99	1087.44
Void calculation T_{fuel} = 1263 K					
$P_{coolant}$ (bar)	k_{eff}	σ_{std}	ρ (pcm)	Δρ (pcm)	
1	1.02294	0.000057	2242.56	326.39	

The behavior of the defined system, which is caused by the change of basic parameters, corresponds to the theoretical assumptions. In the Doppler case, the decrease in k_{eff} represents the negative reactivity feedback, and in the void case, the increase in the k_{eff} corresponds to the positive reactivity change as was expected. The average number of neutrons per fission event was calculated to 2.91 and this value did not change significantly in individual cases. The effective fraction of delayed neutrons was calculated by MCNP5 using the adjoint-weighted point kinetics method [13]. The obtained value for the case with the CSDs and DSDs outside the core was 381 ± 7 pcm. The results of the control rods worth are shown in Table VII.

TABLE VII
WORTH AND EFFICIENCY OF THE CONTROL RODS

Identifier	MCNP5 - CE			KENO6 - MG		
	$\Delta\rho_i^a$ [pcm]		$\Delta\rho_i^r$ [pcm]	$\Delta\rho_i^a$ [pcm]		$\Delta\rho_i^r$ [pcm]
	Hom.	Het.		Hom.	Het.	
All down	12364	11273	0.912	12333	11259	0.913
DSD	4367	4010	0.918	4317	3972	0.920
CSD	8016	7234	0.902	8014	7259	0.906
CSD1R	1472	1352	0.919	1438	1329	0.925
CSD2R	4640	4303	0.927	4629	4299	0.929
CSD2	305	265	0.866	291	260	0.894
CSD3	309	265	0.855	292	260	0.889
CSD10	255	239	0.938	249	241	0.968
CSD11	274	243	0.886	253	236	0.933
DSD0	303	269	0.890	297	260	0.876
DSD4	299	264	0.883	296	274	0.926
DSD5	302	269	0.890	298	269	0.903

The average deviation between MCNP and KENO was 394 pcm and it was almost constant in each case. This difference may have been caused by the multi-group treatment of KENO 6. The efficiency of the heterogeneous CR design was calculated as a ratio of the CR worth for heterogeneous and homogenous designs. The MCNP calculations showed the efficiency of all control rods inserted in the core (ALL_DOWN) of a value 0.912. The highest efficiency was found in case of the CSD10 position (0.938) and the lowest value in case of CSD3 (0.855). There is a good agreement between the MCNP and SCALE6 results. The total worth of all heterogeneous safety devices was calculated to 11273 pcm (11259 pcm), the worth of the CSD devices 7234 pcm (7259 pcm) and the worth of DSD devices 4010 pcm (3972pcm). The values in brackets were obtained from the KENO6 calculations.

B. Amplification Factors

The shadowing and anti-shadowing effects of the control rods were investigated through the calculations of amplification factors, by means of (10) In this equation $\Delta\rho_{1,2..N}$stands for the worth of all devices, $\Delta\rho_i$for the worth of the investigated device and $\Delta\rho_{(1,2..N)-i}$ for the total worth of control devices expect the investigated one. The results are shown in Table VIII. If A_i>1, the CR worth is amplified, and this corresponds to an anti-shadowing effect, while if A_i<1, the CR worth is reduced and one has a shadowing effect.

$$A_i = \frac{\Delta\rho_{1,2..N} - \Delta\rho_{(1,2..N)-i}}{\Delta\rho_i} \quad (10)$$

TABLE VIII
THE EVALUATED AMPLIFICATION FACTOR OF THE CONTROL RODS

Identifier	MCNP		KENO
	Hom.	Het.	Het.
DSD	0.998	1.004	1.004
CSD	0.998	1.004	1.004
CSD1R	0.809	0.862	0.849
CSD2R	1.629	1.586	1.500
CSD2	0.415	0.494	0.361
CSD3	0.375	0.494	0.337
CSD10	10.087	8.839	9.045
CSD11	7.205	6.718	7.041
DSD0	0.206	0.347	0.191
DSD4	1.661	1.756	1.576
DSD5	1.308	1.368	1.289

Considering the heterogeneous CR design, the amplification factors of single devices show shadowing effects in case of CSD2,3 and DSD0 devices and intermediate anti shadowing effect in case of DSD4,5 devices. Similar behaviour was also observed in case of homogenous design. The strongest anti shadowing effect in the heterogeneous design was found for devices CSD10,11 where the amplification factors reached the values of 8.839 (9.045) and 6.718 (7.041) respectively. This effect was even stronger in case of the homogenous configuration due to bigger overall weight of the interacting control rods.

C. Reflector Withdrawal

In this section the *LMF* factor defined in the section IV is used to determine multiplication capabilities of each S/A in the area of interest. If the *LMF* and neutron flux is evaluated, some specific areas in the outer fuel region which can be called "hot spots" can be localized; see Fig. 8. In the centre of these areas, *LMFs* are very close to unity or their value is slightly more than one. In some special cases it can be interpreted that these regions are able to produce more neutrons in the next generation as was born in previous generation.

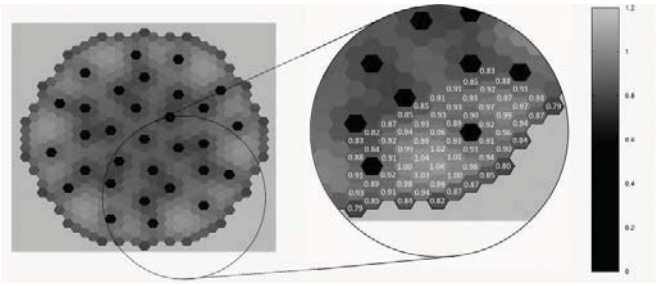

Fig. 8 Spatial distribution of *LMF* in "All down" case

The occurrence of these hot spots was confirmed also by spatial neutron flux distribution; see Fig. 11 (a).

As was proposed in [5], one way to reduce or eliminate these hot spots is to withdraw the first reflector ring. By this way, we can increase a leakage of the neutrons from the reflector-fuel boundary area. This behavior can be seen in Fig. 11 (b) where the hot spot areas are smaller and penetration of neutrons to reflector zone is deeper. For *LMF*, some reduction is reached but not such a significant as with homogeneous CSD and DSD design. Fig. 9 shows *LMFs* for S/A with values close to unity. S/A close to CSD, DSD and reflector are safely sub-critical, but their spatial impact was truncated by use of heterogeneous DSD and CSD design. This effect can lead to the formation of sharp peaks in the centre of hot spots.

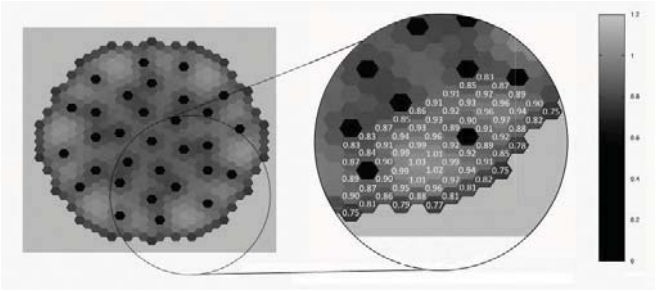

Fig.9 Spatial distribution of *LMF* in "All down" case with 1st reflector ring withdrawn

To obtain similar impact as was obtained by CSD and DSD homogeneous design [5], withdrawal of the second reflector ring was investigated. Strong effect of neutron leakage is evident; see Figs. 10 and 11 (c), but in some parts, the neutron flux reached a reflector edge.

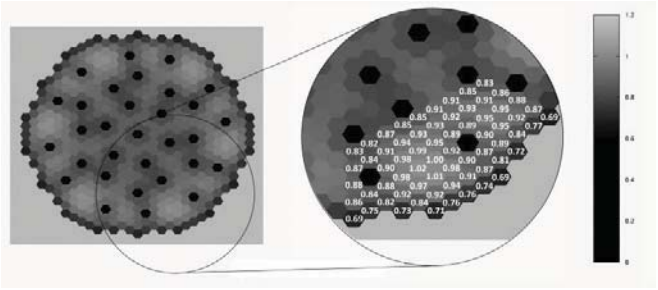

Fig.10 Spatial distribution of *LMF* in "All down" case with 1st and 2nd reflector ring withdrawn

To maintain shielding capabilities of external structures of the core, using the second reflector ring should be more thoroughly deeper investigated. Still, the overall impact to *LMF* was proved; see Figs. 10 and 11 (c). *LMF* of some S/A in hot spots are still more than unity, but the total number of S/A with *LMF* below this threshold was increased.

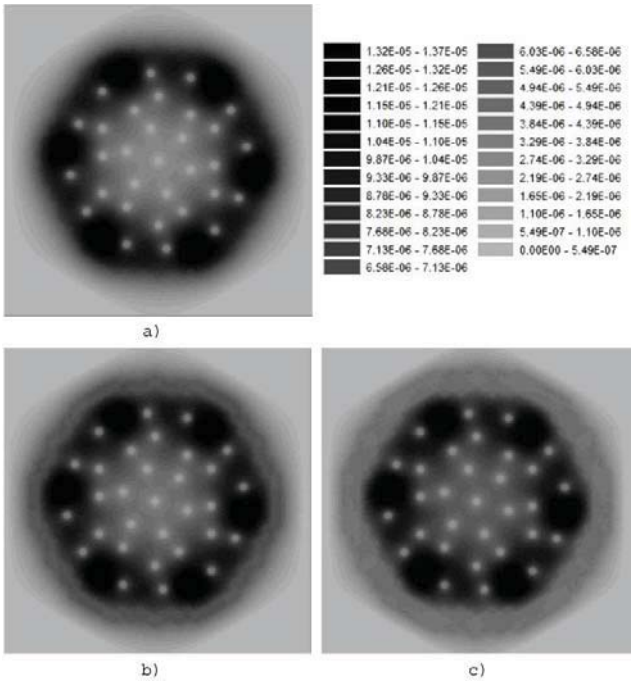

Fig.11 The spatial distribution of neutron fluxes for (a) "All down" case, (b) "All down" case with 1st reflector ring and (c) "All down" case with 1st and 2nd reflector ring

VII. Conclusion

GFR2400 is promising ceramic fuel pin core design. Due to the fact that the development is not finalized, the important part of the core, as the CRs are, was defined just in homogeneous way. Therefore this paper describes the methodology of developing heterogeneous configuration in effective manner, and for selected design heterogeneity effects were investigated. The works were divided into three steps where within these steps new parameters describing calculated results were developed. In the first step, based on investigation of the optimal absorber pin diameter in terms of economic utilization of absorber material, the promising configuration of absorber pin in 5 and 6 rings were identified. In the second step the optimization was aimed to identify effective absorber pin diameter based on optimal number of rings. Within this step the consideration of 5 or 6 rings as an optimal configuration was proved. Since the results from single-pin and ring-wise investigations were in a good agreement, 5 ring configuration was selected as basic design in this analyses. For this design in the third step the optimal pin pitch was found where the self-shielding effect between adjacent absorber pins was investigated. Based on these results the basic design was defined as 5 ring configuration with 1.9 absorber pin pitch and was used in subsequent calculations.

For the basic design of CR implemented to the core of GFR2400 main parameters like worth, efficiency or amplification factor were determined. At the beginning, Doppler and void coefficients were calculated. Due to fact that all CRs are in their upper position influence on these two coefficients is minimal. Results from Doppler and void calculation are in agreement with those performed before. Control rod worth calculated by both codes are consistent. Small differences can be observed but all of them are within statistical uncertainty. Compared to CR worth for homogeneous design, efficiency of investigated cases fulfilled our expectations. In all cases the efficiency was less then unity but did not exceed value less than 0.88. Good agreement was also achieved between KENO6 and MCNP results. The results from CR shadowing calculation are showing that there is almost no interaction between the CSD and DSD systems for both homogenous and heterogeneous design; however, slight interference can be seen between the first and the second ring of the CSD system. Significant shadowing or anti-shadowing effects were observed just for individual CRs. Comparison between amplification factors for heterogeneous and homogeneous designs of CR showed a good consistency which was confirmed by KENO6 calculation. The last part deals with spatial effectiveness of CR. In the GFR2400 core local hot spots were localized where LMF are over unity. Third reactivity control system, which uses the removal of the first and second reflector ring, is able to reduce this effect as well as with homogeneous CR but still it is not sufficient.

Developed methodology within this analysis identifies heterogeneous CR design which met all attributes emerging from homogenous design thus confirm their reliability and in future can be used in development of final control rod design not only for fast reactors.

ACKNOWLEDGMENT

This study was supported by the Slovak Research Development Agency No. APVV-0123-12. Authors would like to thank to all GoFastR project participants for valuable advice.

REFERENCES

[1] Forum, U.S. DOE Nuclear Energy Research Advisory Committee and the Generatio IV International, "A Technology Roadmap for Generation IV Energy Systems," 2002.
[2] P. Anzieu, R. Stainsby and K. Mikityuk, "Gas-cooled Fast Reactor (GFR): Overview an Perspektives," in *GiF Symposium*, Paris, 2009.
[3] Z. Perko, S. Pelloni, K. Mikityuk, J. Kreppel, M. Sziebert, G. Geatan, B. Vrban, J. Luley, Š. Čerba, M. Halasz, S. Feher, T. Reiss, J. L. Kloosterman, R. Stainsby and C. Poette, "Core Neutronic Characterization of the GFR2400 Gas Cooled Fast Reactor," *Progress in Nuclear Energy,* submitted for publication.
[4] GoFastR, "GFR 2400 MWth pin core at start of GOFASTR". Internal document
[5] B. Vrban, Š. Čerba, J. Lüley, J. Haščík, V. Nečas and S. Pelloni, "Investigation of the Coupled Reactivity Effects of the Movable Reflector and Safety Control Rods in the GFR," in *Proceedings of International Conference on Fast Reactors and Related Fuel Cycles: Safe Technologies and Sustainable Scenarios*, Paris, 2013.
[6] M. Zabiego, C. Sauder, P. David, G. C., L. Briottet, J. J. Ingremeau, A. Ravenet, C. Lorrette, L. Chaffron, P. Guédeney, M. Le Flem and J. Séran, "Overview of CEA's R&D on GFR fuel element design: from challenges to solutions," *Progress in Nuclear Energy,* 2014, submitted for publication.
[7] W. van Rooijen and J. Kloosterman, "Closed Fuel Cycle and Minor Actinide Multirecycling," *Science and Technology of Nuclear Installations,* 2009.
[8] ORNL, "SCALE: A Comperhensive Modeling and Simulation Suite for Nuclear Safety Analysis and Design," 2011.
[9] LANL, "MCNP X-5 MONTE CARLO TEAM: MCNP - A General N - Particle Transport Code," 2003.
[10] G. Girardin, G. Rimpault, F. Morin, J. C. Bosq, P. Coddington, K. Mikityuk and R. Chawla, "Development and characterization of the control assembly system for the large 2400 MWth Generation IV gas-cooled fast reactor," *Annals of Nuclear Energy,* no. 35, pp. 2206-2218, 2008.
[11] R. MacFarlane and D. W. Muir, "The NJOY Nuclear Data Processing System," 1994.
[12] Y. Katoh, D. F. Wilosn and C. W. Forsberg, "Assesment of Silicon Carbide Composites for Advanced Salt-Cooled Reactors," 2007.
[13] B. C. Kiedrowski, F. B. Brown and P. P. H. Wilson, "Calculating Kinetics Parameters and Reactivity Changes With Continous-Energy Monte Carlo".

Ján Haščík was born in Zilina, Slovakia (07.121944). In 1970 he graduated from the Moscow Power Engineering Institute (Technical University), in the area of nuclear installations. Since 1970 he has worked at the Department of Nuclear Physics and Technology, Faculty of Electrical Engineering and Information Technology of Slovak University of Technology (FEEI SUT) as a senior lecturer. He gained the PhD degree (2005) from FEI STU in area Investigation of Radiation Degradation of Reactor Pressure Vessel Steels and degree of associated professor (2006) in Nuclear Power Engineering.

The main field of his research and teaching activities is Theory of Nuclear Reactors, Experimental Reactor Physics, Application of Spectroscopic methods for investigation of materials used in nuclear industry (about 100 original papers in scientific journals or at international conferences and he has approx. 20 citations).

Assoc. Prof. Ján Haščík, PhD. is also member of Examination board of Nuclear Regulatory Authority of Slovak Republic for Verification of Specific Abilities of Operating Staff of Nuclear Power Plants in Slovakia. Since 2002 he is responsible for a Periodical training for NPP supervising physicists on Reactor physics experiments. At frame of ENEN from 2003 he has actively participated at organization of E. Wigner Course for Reactor Physics Experiments.